



# Geophysical Research Letters

## RESEARCH LETTER

10.1029/2019GL086248

### Key Points:

- The “Warm Arctic-Cold Siberia” (WACS) pattern is an internal mode of variability, which cannot be excited by GHGs and solar forcing
- Observational and simulated results suggest that the frequent occurrence of the WACS pattern is instigated by the warm phase of AMO
- Warm Atlantic generates an Atlantic-Eurasian wave train that enhances Ural Mountain ridge and East Asian trough, causing the WACS pattern

### Supporting Information:

- Supporting Information S1

### Correspondence to:

B. Wang, and J. Liu,  
wangbin@hawaii.edu;  
jliu@njnu.edu.cn

### Citation:

Jin, C., Wang, B., Yang, Y.-M., & Liu, J. (2020). “Warm Arctic-cold Siberia” as an internal mode instigated by North Atlantic warming. *Geophysical Research Letters*, 47, e2019GL086248. <https://doi.org/10.1029/2019GL086248>

Received 1 DEC 2019

Accepted 10 APR 2020

Accepted article online 17 APR 2020

## “Warm Arctic-Cold Siberia” as an Internal Mode Instigated by North Atlantic Warming

Chunhan Jin<sup>1</sup> ID, Bin Wang<sup>2,3</sup> ID, Young-Min Yang<sup>3</sup> ID, and Jian Liu<sup>1,4</sup> ID

<sup>1</sup>Key Laboratory for Virtual Geographic Environment of Ministry of Education/State Key Laboratory Cultivation Base of Geographical Environment Evolution of Jiangsu Province and Jiangsu Center for Collaborative Innovation in Geographical Information Resource Development and Application, School of Geography Science, Nanjing Normal University, Nanjing, China, <sup>2</sup>Department of Atmospheric Sciences and International Pacific Research center, School of Ocean and Earth Science and Technology, University of Hawaii at Manoa, Honolulu, Hawaii, USA, <sup>3</sup>Earth System Modeling Center, Nanjing University of Information Science and Technology, Nanjing, China, <sup>4</sup>Jiangsu Provincial Key Laboratory for Numerical Simulation of Large Scale Complex Systems, School of Mathematical Science, Nanjing Normal University, Nanjing, China

**Abstract** Eurasia has experienced more frequent bitter winters over the past two decades, which concurred with a prominent “Warm Arctic-Cold Siberia” (WACS) pattern that is unexpected from global warming. Here we show, by analysis of 117-year observations and climate model’s millennial simulations, that the WACS is an internal mode of winter temperature variability, which cannot be excited by greenhouse gases and solar forcing. Observational and simulated results suggest that frequent occurrences of that WACS pattern are instigated by warm phases of Atlantic Multidecadal Oscillation (AMO). North Atlantic warming may activate the WACS by generating a background Atlantic-Eurasian wave train characterized by enhanced Ural Mountain ridge and East Asian trough, which is conducive to recurrent WACS pattern. The wave train-induced the Barents Sea ice melting can act as an amplifier, reinforcing the WACS. Although increased greenhouse gases favor a uniform warming pattern, they may contribute to WACS formation by affecting AMO.

**Plain Language Summary** During the past two decades, Eurasia has experienced frequent bitter winters against the rapid warming over the Arctic, which have caused severe damage to livelihoods and socio-ecological systems. The prevailing paradigm attributes cold Eurasia to accelerated Barents-Kara Sea ice melt as part of global warming. Here we show, by analysis of 117-year observations and climate model’s millennial simulations, that the WACS is an internal mode of winter temperature variability instigated by a warm phase of Atlantic Multidecadal Oscillation (AMO). North Atlantic warming stimulates the WACS by generating a background planetary wave train that is conducive to the frequent occurrence of the WACS. Although increased greenhouse gases favor a uniform warming pattern, they may contribute to WACS formation by affecting AMO. The findings deepen our understanding of the interactive influences of natural variability and anthropogenic forcing on climate change and shed light on future change of northern winter climate under increasing anthropogenic forcing.

## 1. Introduction

Over the latest two decades, adverse cold winters have occurred more frequently than before in Eurasia (Cohen et al., 2012; Mori et al., 2014), which is concurrent with pronounced warming over the Arctic, especially over the Barents-Kara sea region. This “warm Arctic-cold Siberia (or Eurasia)” (WACS) pattern has attracted prodigious attention in the climate research community because such unexpected cold winters in Eurasia have caused severe damage to livelihoods and socio-ecological systems (Nandintsetseg et al., 2018) and have unexpectedly interrupted the anthropogenic forcing-induced global warming trend.

The origin of the WACS phenomenon remains largely unknown regardless of years of debate. Majority of the existing studies attribute the Siberia cooling to a rapid decline in the Arctic sea ice over the Barents-Kara sea region as part of the global warming (Cohen et al., 2012; Inoue et al., 2012; J. Liu et al., 2012; Mori et al., 2014; Nandintsetseg et al., 2018; Tang et al., 2013). Explanations of the physical processes leading to the Siberian cooling are divided into two schools of thought. The first school postulates a stratospheric pathway or stratosphere-troposphere coupling. The Arctic warming induces a weakening or a shift of the

© 2020. The Authors.

This is an open access article under the terms of the Creative Commons Attribution License, which permits use, distribution and reproduction in any medium, provided the original work is properly cited.

stratospheric polar vortex (Jaiser et al., 2013; Kim et al., 2014), and a subsequent downward propagating circulation anomaly from the stratosphere to the troposphere generates the WACS pattern (Hell et al., 2020; Nakamura et al., 2016; Screen, 2017; Sun et al., 2015; Zhang et al., 2018). The second school advocates a tropospheric pathway through a direct response of the tropospheric circulation to Arctic warming. The Arctic ice reduction and the associated Arctic warming may cause the Siberia cooling by a number of processes including: (i) enhancing turbulent heat flux that amplifies the Siberian High and causes cold Far East (Honda et al., 2009); (ii) decreasing the poleward temperature gradient that weakens the polar jet stream (Francis et al., 2009) and baroclinic instability, thus preventing transient cyclones traveling eastward, resulting in anomalous anticyclonic winds and leading to a cold Siberia (Inoue et al., 2012); (iii) generating more frequent Ural (or Barents-Kara sea) blocking highs during a positive phase of North Atlantic Oscillation (NAO) that favor for cold-air advection to Eurasia (D. Luo et al., 2016; Wegmann et al., 2018); or (iv) developing anomalous anticyclone over the Ural mountain that further enhances the downstream East Asian trough by Rossby wave dispersion (Kug et al., 2015).

Results from an atmosphere-only model simulation suggest that the sea-ice reduction in the Barents-Kara Sea can double the probability of severe winters in central Eurasia (Mori et al., 2014). However, the atmosphere-ocean-sea ice coupled climate models' ensemble results suggest that the sea-ice-driven cold winters are unlikely to dominate a future warming climate (McCusker et al., 2016; Mori et al., 2014). In this context, the recent cold Eurasian events could be a consequence of the natural variability of the atmosphere (McCusker et al., 2016; Sun et al., 2016), but how the internal variability causes the WACS was unanswered. Observations show that the uniform cold Siberia pattern is the leading mode of interannual variations of the Asian winter monsoon, which is preceded by a Barents Sea warming in the previous autumn; while on the decadal time scale, cold Siberia is unrelated to Arctic warming (Luo & Wang, 2018). Does the WACS pattern represent a response to the external forcing, such as greenhouse gases or solar radiation, or a form of internal variability, or a combination of the two? A more important issue is: What determines the WACS dynamics in the absence of external forcing, such as greenhouse gases and solar radiation?

## 2. Observational Datasets and Numerical Experiments

Our analysis used several reanalysis datasets. The monthly mean reanalysis data from ERA-20C during the period 1900–2010 (Poli et al., 2013), ERA-40 over the period 1958–2002 (Uppala et al., 2005), and ERA-Interim over the period 1979–2018 (Dee et al., 2011) were obtained from the European Centre for Medium-Range Weather Forecasts. To make these datasets consistent, we first combined ERA-40 (1958–1978) and ERA-Interim (1979–2017) by adjusting the mean state of the ERA-40 data based on the monthly climatology of the ERA-Interim during the overlap period (1979–2001). The resultant dataset (1958–2017) is further merged with the ERA-20C (1900–1957) by removing the differences in monthly climatology during the overlap period (1958–2010) from the ERA-20C dataset. Hereafter, we refer the new dataset as Merged ERA20C reanalysis. The AMO index is obtained from the KNMI Climate Explorer, which was derived from the Hadley Centre Sea-Surface Temperature (HadSST.4.0.0.0) dataset ([https://climexp.knmi.nl/getindices.cgi?WMO=UKMOData/amo\\_hadsst&STATION=AMO\\_hadsst&TYPE=i&id=someone@somewhere](https://climexp.knmi.nl/getindices.cgi?WMO=UKMOData/amo_hadsst&STATION=AMO_hadsst&TYPE=i&id=someone@somewhere)).

The numerical simulation data were obtained from Community Earth System Model-Last Millennium Ensemble (CESM-LME) modeling project for the period of AD 850–2000 (Otto-Bliesner et al., 2016). The LME outputs used here include one control (CTRL) experiment, four solar-only forcing experiments, and three greenhouse gases (GHGs)-only forcing experiments. In the CTRL experiment, with external forcing fixed at the AD 50, the climate variations arise solely from the internal variability within the Earth's coupled climate system. In the four solar-only experiments, changes in the total solar irradiance (TSI) were prescribed according to the reconstructed solar forcing (Vieira et al., 2011). In the three GHGs experiments, the varying greenhouse gases ( $\text{CO}_2$ ,  $\text{GH}_4$ , and  $\text{N}_2\text{O}$ ) deduced from the high-resolution Antarctic ice cores were applied (Schmidt et al., 2011). All other external forcings were fixed at the conditions of AD 850 for each single-forcing simulation. The analyses of the two sets of single-forcing experiments are based on their corresponding ensemble mean results, which, for simplicity, are referred to as solar-only and GHGs-only experiments, respectively.

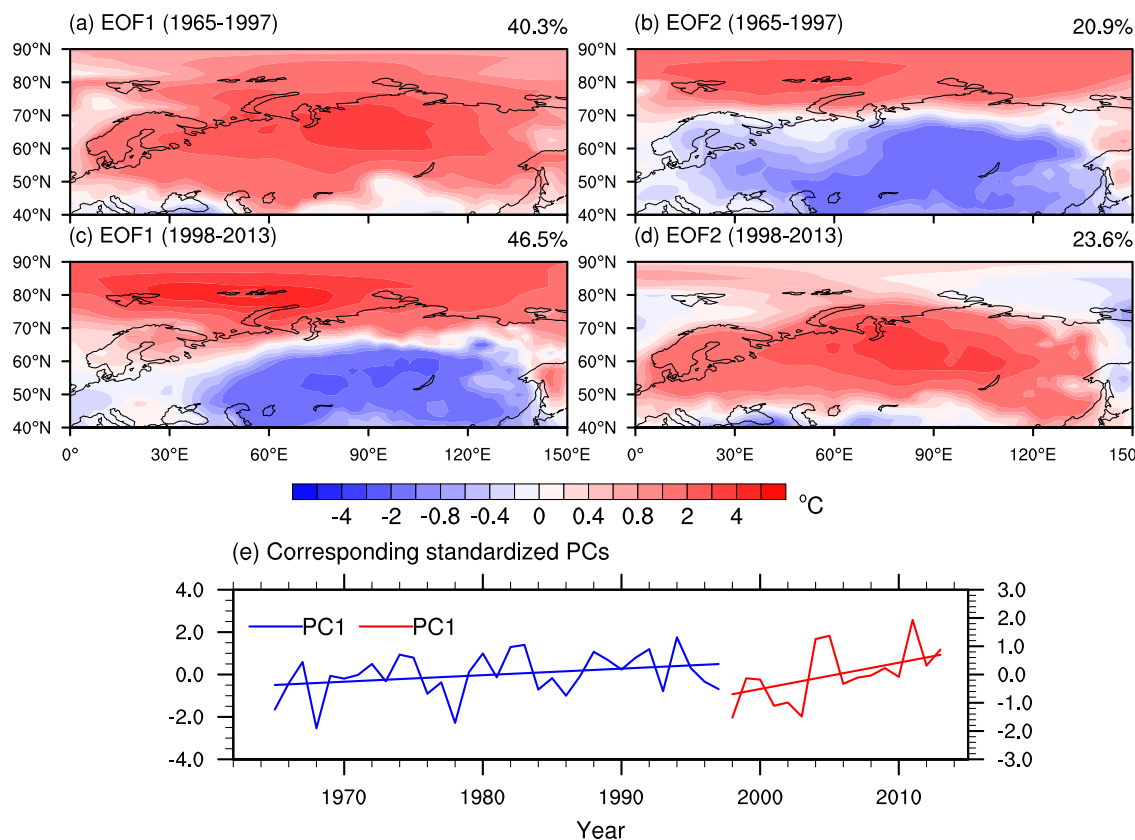


**Figure 1.** Two major EOF modes of the DJF mean surface air temperature (a) and (b) during 1965–1997 and (c) and (d) during 1998–2013 derived from the merged ERA20C reanalysis data. (e) the corresponding standardized PC1s of the EOF modes. The straight lines denote trend lines. Only the PC1 over 1998–2013 is significant at the 95% confidence level using a two-tailed Student's *t*-test.

### 3. Results

#### 3.1. The Nature of the Observed WACS Pattern

We note that the winter (December to February, DJF) mean surface air temperature (SAT) averaged over the Barents-Kara Sea region ( $70\text{--}82^\circ\text{N}$ ,  $0\text{--}70^\circ\text{E}$ ) has a positive trend since 1965, in which anthropogenic radiative forcing is likely to have played a role. However, the SAT over northern Eurasia ( $40\text{--}60^\circ\text{N}$ ,  $50\text{--}130^\circ\text{E}$ ) experienced a multidecadal variation with a “trend” reversal around 1998 and 2013 (Figure S1). Results here suggest that the recent emergence of the WACS pattern may be partially related to the multidecadal variation.

To reveal the nature of the trend reversal around 1998, we performed an empirical orthogonal function (EOF) analysis of the winter SAT over the Arctic-northern Eurasia region for the epochs of 1965–1997 and 1998–2013, separately. The two major EOF patterns during both epochs are significantly separated from other EOF patterns by testing the statistical significance of the sampling error (North et al., 1982). During the pre-1997 epoch, the first EOF mode (EOF1) displays a uniform warming pattern with a fractional variance of 40.3%, and the second EOF mode (EOF2) shows a dipolar WACS pattern (Figure 1). Interestingly, during the 1998–2013 epoch, the WACS pattern becomes the leading mode that explains 46.5% of the total variance, while the uniform warming pattern becomes the EOF2 with reduced fractional variance. The standardized first principal components (PC1s) during 1998–2013 feature a significant increasing trend (Figure 1(e)). The results indicate that during 1965–1997, the SAT is dominated by the uniform warming mode, while after 1997, it is overwhelmed by the WACS mode, which suggests that the trend changed around 1998 and essentially linked to the change in the leading mode of the SAT variability.

#### 3.2. Impacts of the External Forcing

While the WACS is an internal EOF mode of climate variability, it can arguably be affected by external forcing. Here we first examine the trend patterns induced by various external forcing with the CESM-LME

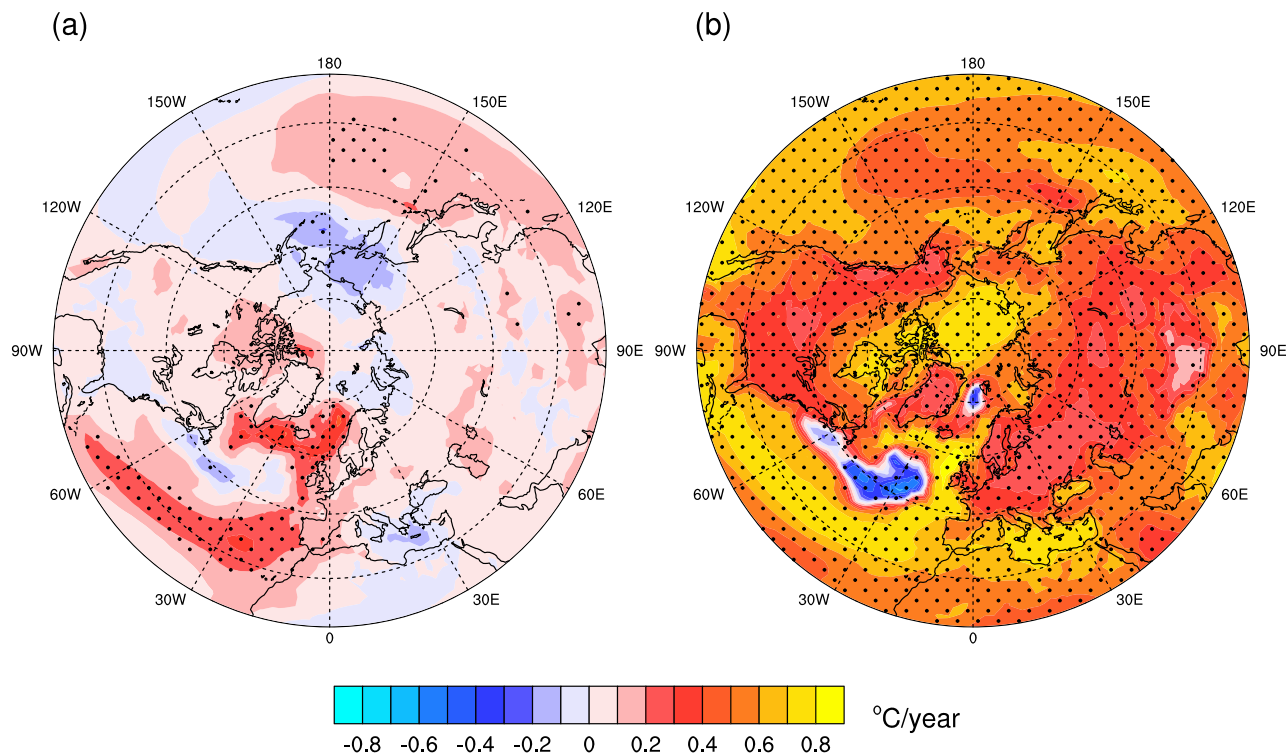


**Figure 2.** Spatial patterns of the linear trends in DJF surface air temperature during the present-day warming period (1850–2000) derived from (a) solar-only experiment, and (b) GHGs-only experiment. The dotted areas are significant at the 95% confidence level, which is conducted by a two-tailed  $r$ -test.

simulation data. Because volcanic eruptions and land use/land cover induce a cooling in the Northern Hemisphere (Bonan, 2008; Stoffel et al., 2015), we consider only possible influences from two sources of external forcing: solar irradiance and greenhouse gases. During the industrial period (1850–2000), greenhouse gas concentrations increased substantially, while solar forcing also shows an upward trend but with considerable decadal fluctuations (Figure S2). In the solar-only experiment, the SAT exhibits a slight global warming trend pattern but the trend over northern Eurasia is insignificant (Figure 2(a)). In contrast, greenhouse gases induce a conspicuous uniform warming trend pattern (Figure 2(b)). Nevertheless, neither the solar nor greenhouse gas forcing produces a WACS-like trend pattern.

Next, we investigate the responses of the internal modes to external forcing. We compare the simulation results derived from the CTRL with those from the solar-only and GHGs-only experiments during the industrial period. We first identify the major modes of DJF SAT variability simulated in the 900-year CTRL experiment by randomly selecting a 151-year sample. The two major EOF modes of the CTRL experiment explain 29.9% and 24.1% of the total variance, respectively (Figure 3(a), 3(b)). However, the order (importance) of these two modes derived from other 151-year segments in the CTRL experiment can be reversed, suggesting that the two major modes are equally important. How would these two internal modes respond to the solar and GHGs forcing? The results from GHG and solar forcing experiments indicate that both external forcings enhance the uniform warming mode. In particular, under the increasing greenhouse gases the uniform warming mode dominates and explains about 50% of the total variance (Figure 3(a)). Consistent with the strong 11-year cycle (Figure S2), the solar forcing produces significant decadal power spectral peaks in the two modes, which are absent in the CTRL and GHGs-only experiments (Figure 3(b)), which confirms the previous results concerning the solar impacts on the Asian winter monsoon (Jin et al., 2019). Given that the WACS cannot be directly excited by external forcing, what is responsible for the frequent occurrence of the WACS in recent decades?

### 3.3. The WACS Mode Linking to the Atlantic Multidecadal Oscillation (AMO)

We will now present observed evidences to show that the WACS mode is linked to AMO. We note that the change in the leading mode of variability over the Arctic-Eurasia in the late 1990s is nearly concurrent with a

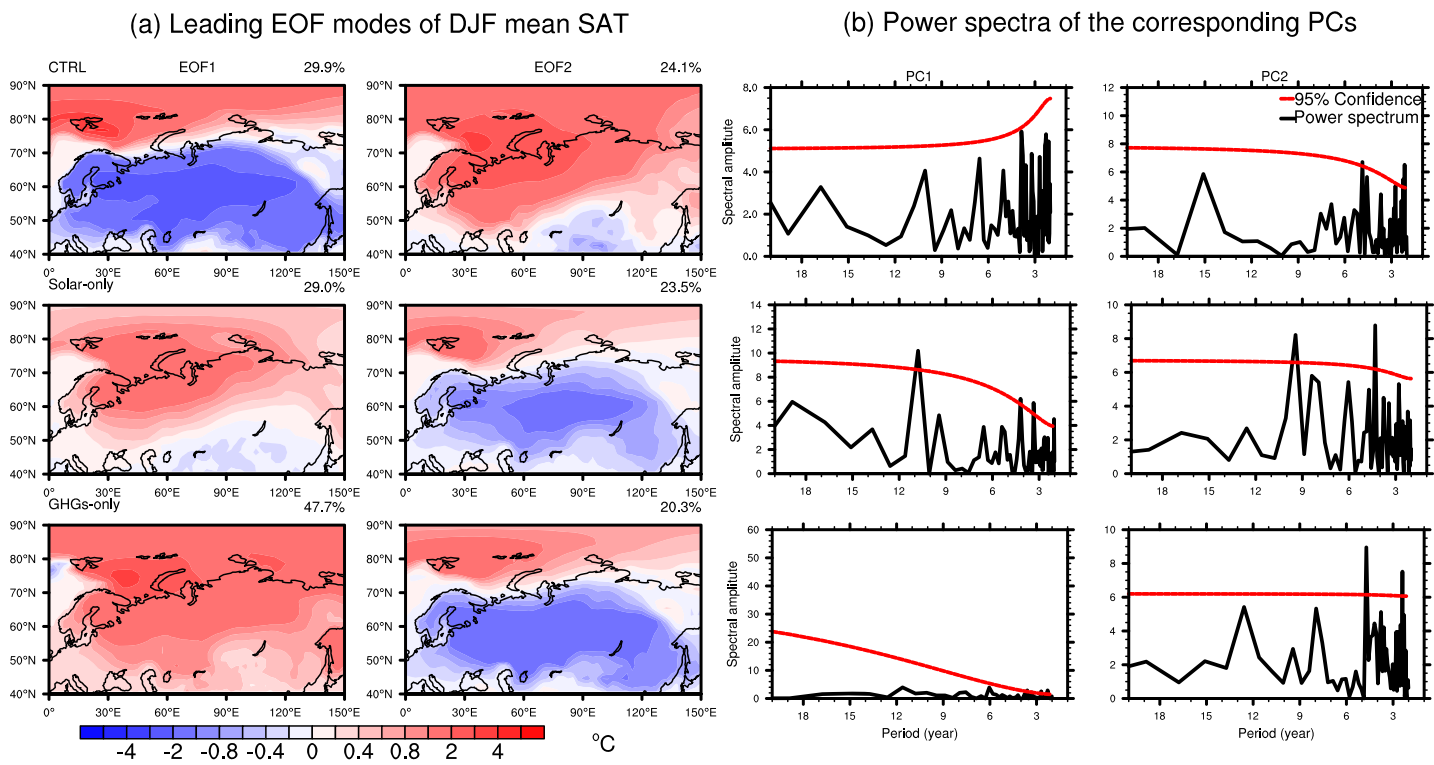


**Figure 3.** (a) Two major EOF modes of the DJF mean surface air temperature derived from the CTRL experiment (upper panel), solar-only experiment (middle panel), and GHGs-only experiment (lower panel). (b) Same as in (a) except for the power spectra of the corresponding PC1s (left panel) and PC2s (right panel). The CTRL is a 151-year segment of the entire CTRL experiment. The solar only and GHG only forcing experiments are for the present warming period (1850–2000).

cold-to-warm phase shift in AMO. Since the beginning of the 20<sup>th</sup> century, the AMO has experienced two negative and two positive phases (Figure 4(a)) (Alexander et al., 2014). To corroborate the linkage between AMO and WACS pattern, we analyze the major modes of the winter SAT over the Arctic-Eurasia during each phase of the AMO since 1900. The leading mode derived for each phase is not affected appreciably by the trend in the data. Note that the leading modes show a uniform pattern during the two negative AMO phases (1901–1926 and 1965–1997) (Figure 4(b), 4(c)). During the two positive AMO phases (1927–1964 and 1998–2013) (Figure 4(d), 4(e)), the leading modes exhibit the WACS pattern, suggesting that the WACS pattern occurs preferably in a warm phase of AMO. It is conceivable that the WACS pattern is stimulated by the warming in the North Atlantic during a positive phase of AMO.

The observed WACS-AMO relationship is further confirmed by the long-term simulations. Given that observation records are not long enough to establish a robust multi-decadal relationship, we examine a 900-year simulation derived from the CTRL experiment. To facilitate analysis, we define a WACS index using the corresponding PC of the simulated WACS pattern. The AMO index is defined as the DJF mean sea surface temperature (SST) anomalies averaged over the northern North Atlantic (25–60°N, 75–7°W) (Van Oldenborgh et al., 2009). As shown in Figure 5(a), the WACS and AMO indices are significantly correlated on the decadal time scale with a correlation coefficient  $r = 0.51$ , the effective degree of freedom is 39 and  $p < 0.05$  by using a two-tailed  $r$ -test (Bretherton et al., 1999).

To further explore why the WACS pattern is enhanced during a positive AMO phase, we selected four strong positive phases of AMO covering a period of 108-years (pink shadings in Figure 5(a)). During the AMO warm phases, the 500-hPa geopotential height exhibits a pronounced Atlantic-Eurasian wave train pattern, which connects a high-pressure center to the west of Azores, a low center over England, a prominent pressure ridge over the Ural Mountains and a northwest-southeast tilted low over East Asia (Figure 5(b)). We have diagnosed the 500-hPa wave activity flux using the method of Takaya and Nakamura (2001). The wave activity flux starts from Azores High, arching across the Atlantic-Eurasian wave train activity centers, indicating that

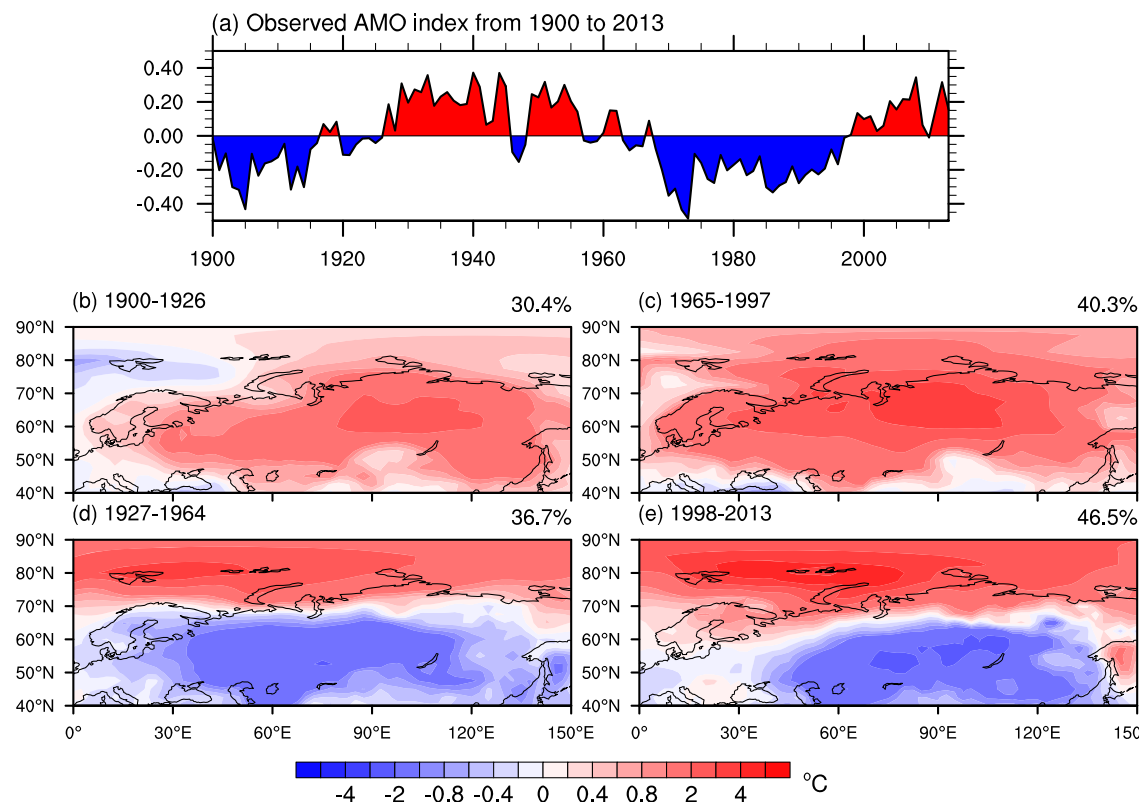


**Figure 4.** The leading EOF modes of the DJF mean surface air temperature during two positive and two negative phases of AMO. (a) Time series of the AMO index obtained from KNMI climate explorer; (b) and (c) the leading EOF modes during two negative phases of AMO (1900–1926 and 1965–1997); (d) and (e) same as in (b) and (c) but for two positive phases of AMO during 1927–1964 and 1998–2013. All EOF1 modes during each phase are significantly separated from the corresponding EOF2 modes.

the wave energy propagation from subtropical North Atlantic contributes to the formation of the Atlantic-Eurasia wave train.

It is important to note that the mean circulation anomalies averaged over a positive phase of AMO (Figure 5(b)) bear close similarity to the interannual circulation anomalies associated with the WACS (Figure 5(c)), especially the characteristic Ural Mountain ridge and East Asian trough. This similarity suggests that the mean circulation anomalies in a warm phase of AMO are conducive to the generation of the WACS pattern. This conclusion derived from model experiments finds support from the result shown in observations. The observed interannual circulation anomalies associated with the WACS (Figure S3a) also resemble the mean circulation anomalies averaged over the warm AMO epoch (1998–2013) (Figure S3b); both are characterized by the Ural Mountain ridge sandwiched by the European and East Asian low pressures. The result here is largely consistent with previous observations that show an AMO warm phase together with a positive NAO can induce persistent Ural blocking events and enhance the transport of moisture into the Arctic (Gimeno et al., 2019; C. Liu & Barnes, 2015), amplifying warming over the Arctic and widespread cooling over Eurasia (Luo et al., 2017).

We note that the wave activity flux tends to increase from the Barents-Kara Sea-Ural Mountain ridge south-eastward, suggesting additional energy propagation from the Arctic to East Asia. To find out the origin of the additional energy source, we examined the sea ice concentration anomalies associated with positive phases of AMO in the CTRL experiment. We find that during a positive phase of AMO, the sea ice in the Barents Sea region declines (Figure S4). The Barents Sea ice melting is likely induced by the Atlantic-Eurasian wave train because the wave train creates an Arctic anticyclone as one of its action centers and the Arctic anticyclone can induce Arctic warming. The Barents Sea warming could further enhance the Ural mountain high and Siberian cooling as indicated by the increased wave activity flux from the Barents Sea to Siberia

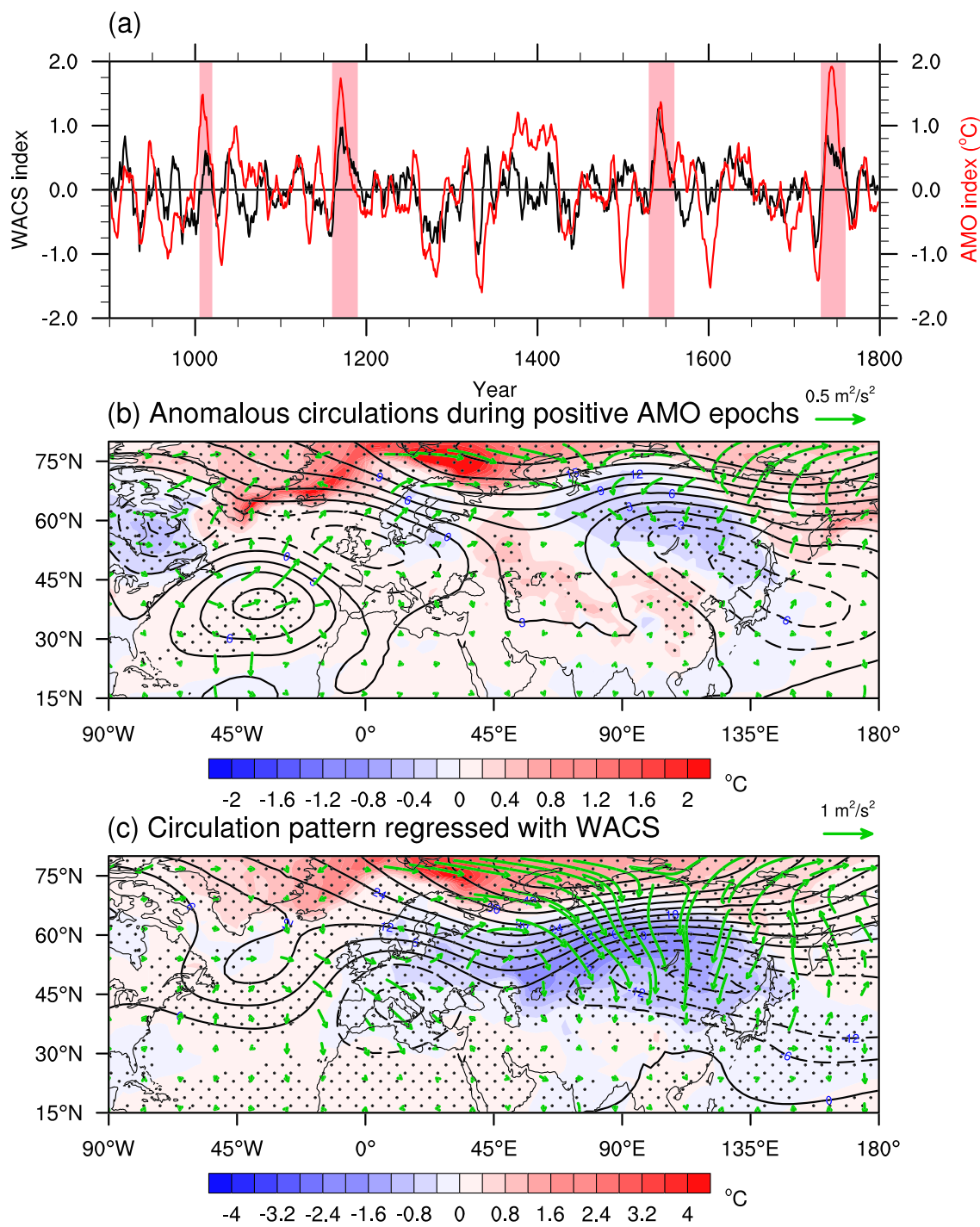


**Figure 5.** The linkage between the WACS and AMO in the model CTRL run. (a) The 11-year running mean time series of standardized WACS index (black line) and AMO index (red line) derived from the CTRL experiment. The pink shadings are used to highlight the epochs with high positive phases of the AMO. (b) Departures (relative to the entire 900-year means) of the DJF mean surface air temperature (color), 500-hPa geopotential height (contour), and 500-hPa wave activity flux (vectors) during the selected positive AMO phases in the CTRL experiment. (c) Circulation anomalies regressed with the WACS index of SAT (color), 500-hPa geopotential height (contour), and 500-hPa wave activity flux (vectors) in the CTRL experiment. The solid (dashed) line represents the positive (negative) pressure. The dotted areas in (b) and (c) are significant at the 90% confidence level. The significant test was performed using a two-tailed Student's *t*-test for panel (b) and a two-tailed *r*-test for panel (c).

(Figure 5(c)) and as shown by the numerical experiments of Kug et al. (2015). The wave train-induced Arctic warming process acts as an “amplifier” to reinforce the WACS occurrence.

#### 4. Conclusion and Discussion

We have shown that the WACS pattern is a major EOF mode of SAT variability over Arctic-northern Eurasia, and the frequent occurrence of the WACS in the recent decades is due to a change in the leading internal mode from the uniform warming to the WACS (Figure 1). We have further shown that the WACS mode cannot be directly excited by the greenhouse gas and solar forcing (Figures 2 and 3), so that it is an internal mode of variability of the coupled climate system. We found that the WACS pattern favorably occurs during warm phases of the AMO in both observation (Figure 4) and the coupled climate model’s millennium simulation (Figure 5). We hypothesize that the positive phases of AMO generate a background Atlantic-Eurasian wave train (Figure 5(b)) that is conducive to the frequent occurrence of the WACS mode (Figure 5(c)). In addition, the wave train can likely induce Barents Sea ice melting as it creates an Arctic anticyclone as one of its action centers (Figure 5(b)). The Barents Sea warming can then act as an amplifier to reinforce the wave train as indicated by the increased wave activity flux from the Barents Sea to Siberia (Figure 5(c)).

Note that the WACS in the recent positive AMO phase (1998–2013) is more prominent than that in the previous positive AMO phase (1927–1965), as indicated by their fractional variances (Figure 4(d), 4(e)). This suggests that anthropogenic forcing or other factors may additionally contribute to the recent amplification of the WACS. One of the possible factors is the rapid ice melting over the Barents-Kara Sea region in recent two decades, which may be partially due to anthropogenic forcing.

Several issues call for future investigation. The first is to find out the precise processes by which North Atlantic warming could cause the sea ice decline over the Barents-Kara Sea region. Secondly, we need to assess the quantitative contributions of the Atlantic-Eurasian wave train and the Arctic reinforcing mechanism to the WACS formation as both are associated with a warm phase of AMO. The third issue is to determine the relative contribution of the AMO and anthropogenic forcing to the recent Arctic warming.

Our findings deepen understanding of the relative influences from natural variability and anthropogenic forcing on the recent climate change and shed light on future change of the northern hemisphere winter climate under the increasing anthropogenic forcing. Our work not only provides insight into the origin of the WACS but also contributes to a potential improvement of the decadal prediction of Eurasian winter temperature and related cold surges. The hypothesis and mechanisms elaborated in this work, however, are based on limited observation and results from a single model simulation. More comprehensive multi-model studies are needed to verify the results. Previous studies have speculated the role of the stratosphere pathway in generating WACS, but the CESM-LME simulation does not have sufficient vertical resolution to test this hypothesis.

#### Data Availability Statements

Data related to this paper can be downloaded from the following.

ECMWF reanalysis, <https://www.ecmwf.int/en/forecasts/datasets/browse-reanalysis-datasets>

AMO index, <http://climexp.knmi.nl/amo.cgi?id=someone@somewhere>

AMO index, <http://climexp.knmi.nl/amo.cgi?id=someone@somewhere>

CESM\_LME, <http://www.cesm.ucar.edu/projects/community-projects/LME/data-sets.html>

External forcings, <http://www.geosci-model-dev.net/4/33/2011/gmd-4-33-2011-supplement.zip>

All the data generated in this analysis will be deposited at the server [clipas.soest.hawaii.edu](http://clipas.soest.hawaii.edu) and are available upon requests.

#### References

- Alexander, M. A., Kilbourne, K. H., & Nye, J. A. (2014). Climate variability during warm and cold phases of the Atlantic multidecadal oscillation (AMO) 1871–2008. *Journal of Marine Systems*, 133, 14–26. <https://doi.org/10.1016/j.jmarsys.2013.07.017>
- Bonan, G. B. (2008). Forests and climate change: Forcings, feedbacks, and the climate benefits of forests. *Science*, 320(5882), 1444–1449. <https://doi.org/10.1126/science.1155121>
- Bretherton, C. S., Widmann, M., Dymnikov, V. P., Wallace, J. M., & Bladé, I. (1999). The effective number of spatial degrees of freedom of a time-varying field. *Journal of Climate*, 12(7), 1990–2009. [https://doi.org/10.1175/1520-0442\(1999\)012<1990:TENOSD>2.0.CO;2](https://doi.org/10.1175/1520-0442(1999)012<1990:TENOSD>2.0.CO;2)

- Cohen, J. L., Furtado, J. C., Barlow, M. A., Alexeev, V. A., & Cherry, J. E. (2012). Arctic warming, increasing snow cover and widespread boreal winter cooling. *Environmental Research Letters*, 7, 14007. <https://doi.org/10.1088/1748-9326/7/1/014007>
- Dee, D. P., Uppala, S. M., Simmons, A. J., Berrisford, P., Poli, P., Kobayashi, S., et al. (2011). The ERA-interim reanalysis: Configuration and performance of the data assimilation system. *Quarterly Journal of the Royal Meteorological Society*, 137(656), 553–597. <https://doi.org/10.1002/qj.828>
- Francis, J. A., Chan, W., Leathers, D. J., Miller, J. R., & Veron, D. E. (2009). Winter northern hemisphere weather patterns remember summer Arctic Sea-ice extent. *Geophysical Research Letters*, 36, L07503. <https://doi.org/10.1029/2009GL037274>
- Gimeno, L., Vázquez, M., Eiras-Barca, J., Sorri, R., Algarra, I., & Nieto, R. (2019). Atmospheric moisture transport and the decline in Arctic Sea ice. *Wiley Interdisciplinary Reviews: Climate Change*, 10, e588. <https://doi.org/10.1002/wcc.588>
- Hell, M. C., Schneider, T., & Li, C. (2020). Atmospheric circulation response to short-term Arctic warming in an idealized model. *Journal of the Atmospheric Sciences*, 77(2), 531–549. <https://doi.org/10.1175/JAS-D-19-0133.1>
- Honda, M., Inoue, J., & Yamane, S. (2009). Influence of low Arctic Sea-ice minima on anomalously cold Eurasian winters. *Geophysical Research Letters*, 36, L08707. <https://doi.org/10.1029/2008GL037079>
- Inoue, J., Hori, M. E., & Takaya, K. (2012). The role of Barents Sea ice in the wintertime cyclone track and emergence of a warm-Arctic cold-Siberian anomaly. *Journal of Climate*, 25(7), 2561–2568. <https://doi.org/10.1175/JCLI-D-11-00449.1>
- Jaiser, R., Dethloff, K., & Handorf, D. (2013). Stratospheric response to Arctic Sea ice retreat and associated planetary wave propagation changes. *Tellus A: Dynamic Meteorology and Oceanography*, 65, 19375. <https://doi.org/10.3402/tellusa.v65i0.19375>
- Jin, C., Wang, B., Liu, J., Ning, L., & Yan, M. (2019). Decadal variability of northern Asian winter monsoon shaped by the 11-year solar cycle. *Climate Dynamics*, 1–10. <https://doi.org/10.1007/s00382-019-04945-4>
- Kim, B.-M., Son, S.-W., Min, S.-K., Jeong, J.-H., Kim, S.-J., Zhang, X., et al. (2014). Weakening of the stratospheric polar vortex by Arctic Sea-ice loss. *Nature Communications*, 5, 4646. <https://doi.org/10.1038/ncomms5646>
- Kug, J.-S., Jeong, J.-H., Jang, Y.-S., Kim, B.-M., Folland, C. K., Min, S.-K., & Son, S.-W. (2015). Two distinct influences of Arctic warming on cold winters over North America and East Asia. *Nature Geoscience*, 8(10), 759–762. <https://doi.org/10.1038/ngeo2517>
- Liu, C., & Barnes, E. A. (2015). Extreme moisture transport into the Arctic linked to Rossby wave breaking. *Journal of Geophysical Research: Atmospheres*, 120, 3774–3788. <https://doi.org/10.1002/2014JD022796>
- Liu, J., Curry, J. A., Wang, H., Song, M., & Horton, R. M. (2012). Impact of declining Arctic Sea ice on winter snowfall. *Proceedings of the National Academy of Sciences*, 109(11), 4074–4079. <https://doi.org/10.1073/pnas.1114910109>
- Luo, D., Chen, Y., Dai, A., Mu, M., Zhang, R., & Ian, S. (2017). Winter Eurasian cooling linked with the Atlantic multidecadal oscillation. *Environmental Research Letters*, 12, 125002. <https://doi.org/10.1088/1748-9326/aa8de8>
- Luo, D., Xiao, Y., Diao, Y., Dai, A., Franzke, C. L. E., & Simmonds, I. (2016). Impact of Ural blocking on winter warm Arctic–cold Eurasian anomalies. Part II: The link to the North Atlantic oscillation. *Journal of Climate*, 29(11), 3949–3971. <https://doi.org/10.1175/JCLI-D-15-0612.1>
- Luo, X., & Wang, B. (2018). Predictability and prediction of the total number of winter extremely cold days over China. *Climate Dynamics*, 50(5–6), 1769–1784. <https://doi.org/10.1007/s00382-017-3720-z>
- McCusker, K. E., Fyfe, J. C., & Sigmond, M. (2016). Twenty-five winters of unexpected Eurasian cooling unlikely due to Arctic Sea-ice loss. *Nature Geoscience*, 9(11), 838–842. <https://doi.org/10.1038/ngeo2820>
- Mori, M., Watanabe, M., Shioigama, H., Inoue, J., & Kimoto, M. (2014). Robust Arctic Sea-ice influence on the frequent Eurasian cold winters in past decades. *Nature Geoscience*, 7(12), 869–873. <https://doi.org/10.1038/ngeo2277>
- Nakamura, T., Yamazaki, K., Iwamoto, K., Honda, M., Miyoshi, Y., Ogawa, Y., et al. (2016). The stratospheric pathway for Arctic impacts on midlatitude climate. *Geophysical Research Letters*, 43, 3494–3501. <https://doi.org/10.1002/2016GL068330>
- Nandintsetseg, B., Shinoda, M., Du, C., & Munkhjargal, E. (2018). Cold-season disasters on the Eurasian steppes: Climate-driven or man-made. *Scientific Reports*, 8, 14769. <https://doi.org/10.1038/s41598-018-33046-1>
- North, G. R., Bell, T. L., Cahalan, R. F., & Moeng, F. J. (1982). Sampling errors in the estimation of empirical orthogonal functions. *Monthly Weather Review*, 110(7), 699–706. [https://doi.org/10.1175/1520-0493\(1982\)110<0699:SEITEO>2.0.CO;2](https://doi.org/10.1175/1520-0493(1982)110<0699:SEITEO>2.0.CO;2)
- Otto-Biesner, B. L., Brady, E. C., Fasullo, J., Jahn, A., Landrum, L., Stevenson, S., et al. (2016). Climate variability and change since 850 CE: An ensemble approach with the community earth system model. *Bulletin of the American Meteorological Society*, 97(5), 735–754. <https://doi.org/10.1175/BAMS-D-14-00233.1>
- Poli, P., Hersbach, H., Tan, D., Dee, D., Thepaut, J.-N., Simmons, A., et al. (2013). The Data Assimilation System and Initial Performance Evaluation of the ECMWF Pilot Reanalysis of the 20th-Century Assimilating Surface Observations Only (ERA-20C). European Centre for Medium Range Weather Forecasts.
- Schmidt, G. A., Jungclaus, J. H., Ammann, C. M., Bard, E., Braconnot, P., Crowley, T. J., et al. (2011). Climate forcing reconstructions for use in PMIP simulations of the last millennium (v1.0). *Geoscientific Model Development*, 4(1), 33–45. <https://doi.org/10.5194/gmd-4-33-2011>
- Screen, J. A. (2017). The missing northern European winter cooling response to Arctic Sea ice loss. *Nature Communications*, 8, 14603. <https://doi.org/10.1038/ncomms14603>
- Stoffel, M., Khodri, M., Corona, C., Guillet, S., Poulin, V., Bekki, S., et al. (2015). Estimates of volcanic-induced cooling in the northern hemisphere over the past 1,500 years. *Nature Geoscience*, 8(10), 784–788. <https://doi.org/10.1038/ngeo2526>
- Sun, L., Deser, C., & Tomas, R. A. (2015). Mechanisms of stratospheric and tropospheric circulation response to projected Arctic Sea ice loss. *Journal of Climate*, 28(19), 7824–7845. <https://doi.org/10.1175/JCLI-D-15-0169.1>
- Sun, L., Perlitz, J., & Hoerling, M. (2016). What caused the recent “warm Arctic, cold continents” trend pattern in winter temperatures? *Geophysical Research Letters*, 43, 5345–5352. <https://doi.org/10.1002/2016GL069024>
- Takaya, K., & Nakamura, H. (2001). A formulation of a phase-independent wave-activity flux for stationary and migratory quasigeostrophic eddies on a zonally varying basic flow. *Journal of the Atmospheric Sciences*, 58(6), 608–627. [https://doi.org/10.1175/1520-0469\(2001\)058<0608:AFOAPI>2.0.CO;2](https://doi.org/10.1175/1520-0469(2001)058<0608:AFOAPI>2.0.CO;2)
- Tang, Q., Zhang, X., Yang, X., & Francis, J. A. (2013). Cold winter extremes in northern continents linked to Arctic Sea ice loss. *Environmental Research Letters*, 8, 14,036. <https://doi.org/10.1088/1748-9326/8/1/014036>
- Uppala, S. M., Källberg, P. W., Simmons, A. J., Andrae, U., Bechtold, V. D. C., Fiorino, M., et al. (2005). The ERA-40 re-analysis. *Quarterly Journal of the Royal Meteorological Society*, 131(612), 2961–3012. <https://doi.org/10.1256/qj.04.176>
- Van Oldenborgh, G. J., Te Raa, L. A., Dijkstra, H. A., & Philip, S. Y. (2009). Frequency-or amplitude-dependent effects of the Atlantic meridional overturning on the tropical Pacific Ocean. *Ocean Science*, 5(3), 293–301. <https://doi.org/10.5194/os-5-293-2009>
- Vieira, L. E. A., Solanki, S. K., Krivova, N. A., & Usoskin, I. (2011). Evolution of the solar irradiance during the Holocene. *Astronomy & Astrophysics*, 531, A6. <https://doi.org/10.1051/0004-6361/201015843>

- Wegmann, M., Orsolini, Y., & Zolina, O. (2018). Warm Arctic— cold Siberia: Comparing the recent and the early 20th-century Arctic warmings. *Environmental Research Letters*, *13*, 25009. <https://doi.org/10.1088/1748-9326/aaa0b7>
- Zhang, P., Wu, Y., Simpson, I. R., Smith, K. L., Zhang, X., De, B., & Callaghan, P. (2018). A stratospheric pathway linking a colder Siberia to Barents-Kara Sea Sea ice loss. *Science Advances*, *4*, eaat6025. <https://doi.org/10.1126/sciadv.aat6025>